Available online at www.sciencedirect.com
ScienceDirect
Earth and Planetary Science Letters 253 (2007) 112–128
EPSL
www.elsevier.com/locate/epsl

# Melting relations in the chloride–carbonate–silicate systems at high-pressure and the model for formation of alkalic diamond–forming liquids in the upper mantle

Oleg G. Safonov [a,*], Leonid L. Perchuk [b], Yuriy A. Litvin [a]

[a] *Institute of Experimental Mineralogy, Russian Academy of Sciences, Chernogolovka, Moscow District, 142432, Russia*
[b] *Department of Geology, Moscow State University, Vorobievy Gory, Moscow, 119899, Russia*

Received 9 June 2006; received in revised form 9 October 2006; accepted 9 October 2006
Available online 17 November 2006
Editor: R.D. van der Hilst

**Abstract**

The experiments in the model system $CaMgSi_2O_6$–($Na_2CO_3$, $CaCO_3$)–KCl are performed at 5 GPa and 1400–1600 °C in order to study the phase relations, including liquid immiscibility, in the chloride–carbonate–silicate systems with application to alkali and chlorine-rich liquids preserved in kimberlitic diamonds. Experiments in the boundary joins of the system demonstrated that both the carbonate–silicate and chloride–carbonate melts are homogeneous; while high-temperature (above 1800 °C) liquid immiscibility is assumed for the chloride–silicate join of the above system. Addition of silicate component into the chloride–carbonate melts and chloride component into the carbonate–silicate melts results in splitting of the homogeneous liquids into the immiscible chloride–carbonate brine and carbonate–silicate melt. Carbonate–silicate and chloride–carbonate branches of the miscibility gap converge within the carbonate-rich region of the system. Regular temperature evolution of the shape and size of the miscibility gap is deduced. With decreasing temperature, the convergence point moves toward more Si-rich compositions, expanding fields of homogeneous chloride–carbonate silica-saturated melts. This effect is governed by the precipitation of the silicate phases even from silica-bearing chloride–carbonate melts. In addition, experiments revealed regular evolution of both Cl-bearing carbonate–silicate melt and Si-bearing chloride–carbonate brine toward the low-temperature chlorine–bearing carbonatitic liquid with decreasing temperature. These trends are similar to the evolution of the melt and brine inclusions in some diamonds from Botswana, Brazil, Canada, and Yakutia, indicating their growth during cooling. The model for interaction of the chloride–carbonate brine with the mantle rocks is developed on the basis of the present experimental data. This model is applied to the chlorine-enriched kimberlites of the Udachnaya–East pipe.


*Keywords:* High-pressure experiment; Chloride–carbonate–silicate melts; Liquid immiscibility; Mantle; Diamonds; Kimberlites

## 1. Introduction

Role of chlorine and alkali chlorides in the formation of mantle rocks is traditionally considered to be negligible (e.g., [1]). Nevertheless, data on compositions of micas, amphiboles, and, especially, apatites from the upper mantle rocks indicate their interaction with fluids enriched in chlorine (e.g. [2–5]). Chlorine-rich fluid inclusions have also been observed in the upper mantle rocks [2,6]. Kimberlites, which are assumed to be derivatives of the most deep-seated mantle melts [7,8],

* Corresponding author. Tel./fax: +7 96 5244425, +7 96 5249687.
*E-mail address:* oleg@iem.ac.ru (O.G. Safonov).

0012-821X/$ - see front matter © 2006 Elsevier B.V. All rights reserved.
doi:10.1016/j.epsl.2006.10.020

provide direct mineralogical and geochemical evidences on presence of alkali chloride compounds during their evolution. Halite and sylvite are known both in groundmass [9] and in secondary melt inclusions in olivine [10] of some fresh Yakutian kimberlites. Recent Sr, Nd, and Pb isotopic study [11] provided strong evidence for primary magmatic origin of alkali chlorides and carbonates in these kimberlites [11]. The deep-seated origin (>4 GPa) of alkali-rich chloride–carbonate liquid as a derivate of kimberlitic magma is supported by the study of primary melt inclusions in olivines from unaltered kimberlites of the Udachnaya–East pipe, Yakutia [12]. The estimated chlorine content of the kimberlite melt, that produces chlorine–carbonate liquid, could be above 7 wt.% [12]. This concentration is much higher than the chlorine solubility in mantle-derived basaltic melts (e.g. [13,14]).

Further evidence for the activity of alkalic Cl-bearing liquids during the evolution of some deep-seated assemblages is provided by the compositions of alkaline (mostly high-potassic) liquid inclusions in diamonds from kimberlites. Four compositional groups of these liquids are distinguished in diamonds from Africa, Canada, Brazil, Yakutia, and India (Fig. 1): (1) alumino–silicate melt inclusions [15–20]; (2) carbonate–silicate melt inclusions [21–27]; (3) carbonate melt inclusions [23,25,27–30]; (4) chloride–carbonate brine inclusions [29–33]. The composition of the brine inclusions in diamonds [29,30,32,33] closely resembles the composition of chloride–carbonate inclusions in kimberlitic olivines [11,12]. Concentration of Cl in the carbonate–silicate inclusions reaches 1.5 wt.% [21–24]. The carbonate-rich inclusions contain 6–12 wt.% of Cl [27–30]. Chlorine in the carbonate–silicate and carbonate inclusions shows a distinct positive correlation with K at negative correlation both with Si and Al (e.g. [22,29,30]). Correlation between K and Cl was previously reported for diamonds from Yakutia, Africa, and Canada, which were analyzed by the proton microprobe, neutron activation method, and step heating techniques [18,34–36]. This correlation implies that KCl is the major chlorine contributor to composition of the above inclusions [30]. Burgess and Turner [36] estimated chlorine content of 2–5 wt.% in the mantle-derived fluid, which is in a good agreement with compositions of carbonate–silicate and carbonate melt inclusions in diamonds. The chloride–carbonate brine inclusions are apparently concentrated in cores of diamond crystals and associated both with eclogitic and peridotitic mineral assemblages [29,32,33]. Locally, products of reactions between mantle minerals and brines are observed in single inclusions in diamonds

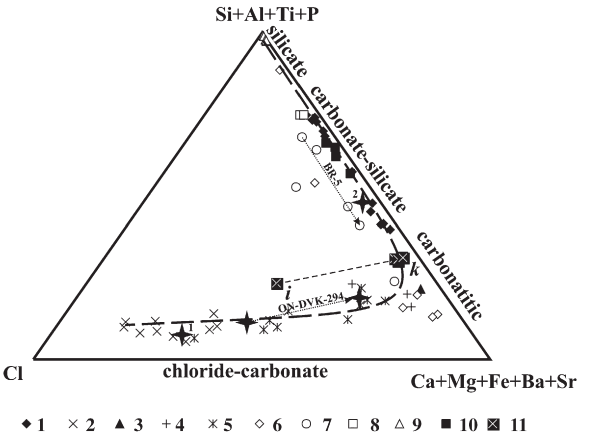


Fig. 1. Variations in compositions of the melt and fluid inclusions in diamonds from kimberlites of (1) Zaire and Botswana [22], (2, 3) Koffiefontein pipe, South Africa [26,32]; (4) Yubileinaya pipe, Yakutia [25,28,30]; (5) Diavik mine, Canada [29,30]; (6) diverse Yakutian pipes (O. Navon, pers. comm.); (7) Brazil [27]; (8) Aikhal pipe, Yakutia [17]; (9) Mir pipe, Yakutia [16,19], as well as (10) from alluvial Indian diamonds (O. Navon, pers. comm.). (11) average composition of chloride–carbonate inclusion in olivine (*i*) and host kimberlites (*k*) from the Udachnaya–East pipe, Yakutia ([11,12], A. Sobolev, pers. comm.). Alkalis are omitted in the diagram since their addition masks behavior of chlorine. Long-dashed thick line illustrates a specific shape of the immiscibility gap in the chloride–carbonate–silicate melts deduced from the composition of the inclusions. Short-dotted thin line shows a tie-line connecting compositions of chloride–carbonate inclusion in olivine (*i*) and host kimberlites (*k*) from the Udachnaya–East pipe, Yakutia, implying their liquid immiscibility relations. Black stars show average compositions of liquids in three diamonds from the Diavik mine [30]: 1 — brine inclusion in diamond ON-DVK-272; 2 — carbonate–silicate melt inclusion ON-DVK-281. Dotted arrows illustrate evolution of average compositions of melt inclusions in diamond BR-5 [27] and ON-DVK-294 [29,30].

[26,30,33]. Assemblage of brine and mineral inclusions allow determination of *P–T* conditions for their entrapment: 4.6–5.1 GPa and 1000–1200 °C [26,32,33]. These data imply that diamond growth was coeval with an influx of alkali-rich chloride–carbonate liquids, which arrived from the greater depths.

Fig. 1 demonstrates regular variations of chlorine in the melts included in diamonds. The data points form two continuous trends along the silicate–carbonate and carbonate–chloride joins [37]. The continuous trend between the silicate and carbonatitic melts is also recorded in compositional variation of the melts inclusions within single diamond crystals [22,27]. Chlorine positively correlates with content of the "carbonate" end-member [22,27]. Brine inclusions from the Koffiefontein pipe [32,33] and the Diavik mine [29,30] also form continuous trends along the chloride–carbonate join. These trends converge near the "carbonate" (Ca + Mg + Fe + Ba + Sr) apex of the diagram

(Fig. 1) with data on Cl-rich carbonatitic inclusions in diamonds [26,28–30] (Fig. 1). According to Navon et al. [37], the continuous trends between the silicate and carbonate inclusions points to perfect miscibility of corresponding melts within the diamond stability P–T conditions. Similar conclusion follows for the chloride–carbonate brines. An absence of data points between silica-rich melts and chloride-rich brines may reflect a wide miscibility gap between them under the upper mantle conditions. Integrating data on compositions of liquid inclusions in diamonds, Klein-BenDavid et al. [38] concluded that carbonate-rich melts were associated both with silica-rich melts and brines, while the carbonate–silicate melts and brines have never been found together in any single diamond. This conclusion supports an idea that the liquid miscibility controls compositions of alkalic liquids trapped in fibrous diamonds. Observation of the chloride–carbonate segregations in unaltered kimberlites of the Udachnaya–East pipe [12] gives an additional evidence for liquid immiscibility between carbonate–silicate (kimberlitic) melts and chloride–carbonate brines within the diamond stability field.

The liquid immiscibility model, tentatively proposed by Perchuk et al. [39] and further developed by Navon et al. [37], might be a powerful tool to explain genetic relations between alkalic Cl-rich melts in the upper mantle. Based on the natural data only, this model never been substantiated experimentally, since liquid immiscibility in the complex chloride–carbonate–silicate systems never been studied at the mantle P–T conditions. Moreover, experimental data on such systems at low pressures are extremely scarce, as well [40–42].

Our paper describes results of experiments on phase relations in the model chloride–carbonate–silicate system $CaMgSi_2O_6$–($Na_2CO_3$, $CaCO_3$)–KCl at 5 GPa. The choice of the boundary components is based on the natural data on melt inclusions in diamonds. KCl is the major chlorine-contributing component in the liquid inclusions preserved in diamonds [22,29,30,32], while Na and Ca are mostly bound into carbonates [30]. Diopside is a major end-member of pyroxenes, which are characteristic phases both for peridotitic, eclogitic, and webstritic deep-seated assemblages. In addition, the above composition of the system allows comparison with experiments at low pressure [41,42].

## 2. Starting materials, experimental technique, and analytical procedures

Mixtures of diopside glass with crystalline $CaCO_3$, $Na_2CO_3$, and KCl were used as starting materials. Four basic chloride–carbonate mixtures (mix. 1, mix. 2, mix. 3, and mix. 4 in Supplementary Table 1) and one basic carbonate–silicate mixture (mix. 5 in Supplementary Table 1) were prepared for the experiments in the ternary system. Desired proportions of either diopside or KCl were added in these mixtures, respectively. About of 20 mg of each mixture were placed into Pt or $Pt_{60}Rh_{40}$ capsules and subsequently dried at 110 °C.

Experiments (Supplementary Table 1) were performed at 5 GPa and 1400–1600 °C with the high-pressure toroidal "anvil-with-hole" apparatus [43–45], which is a modification of the Bridgmen-type anvil assembly [46]. The apparatus is characterized by a homogeneous distribution of pressure and temperature (~1 °C/mm.) in the reaction volume of 0.1–0.15 $cm^3$ (see details in [43]). The limestone high-pressure cell prepared individually for each run is equipped with a graphite heater of 7.2 mm in length, 7.5 mm in diameter, and 0.75 mm wall thickness [43–45]. The capsule was placed in the center of the cell on the holders made of pressed MgO and BN mixture (MgO:BN=3:1). Pressurization of the cell was accomplished using the uni-axial compression of upper and lower anvils in a 500-ton hydraulic press. Pressure at room temperature was calibrated using bismuth phase transitions at 2.55 (Bi I–Bi II), 2.7, and 7.7 (Bi III–Bi V) GPa, as well as barium phase transition at 5.5 GPa [47]. Pressure was corrected for high temperature with the diamond–graphite curve [48] using growth/dissolution of diamond seeds in carbon-oversaturated multicomponent carbonate melts [49]. As a result, run pressure was controlled to ±0.2 GPa. Because of small reaction volume, experiments with the "anvil-with-hole" assembly were not monitored directly with thermocouples. The current power setting control of temperature has been used [43]. The temperature-current power dependence of the cell was calibrated using a $Pt_{70}Rh_{30}/Pt_{94}Rh_6$ thermocouple without pressure correction. The cells were recalibrated after several runs to check the reproducibility of the temperature–current power dependence. Run temperature was controlled within ±20 °C using a MINITHERM-300.31 controller. This accuracy includes an error of the $Pt_{70}Rh_{30}/Pt_{94}Rh_6$ thermocouple used in calibration, self-accuracy of the controller, and an error resulted from the thermogradient in the cell [43]. Duration of each experiment varied in dependence on temperature (Supplementary Table 1). Experiments were quenched by shutting power off and subsequently depressurized. In order to confirm a reproducibility of the experimental results, some paired (similar composition and temperature) experiments were performed (Supplementary Table 1). Experiments 1/1236 and 1498 were carried out using well calibrated various "anvil-with-hole" apparatuses.

Each run sample was embedded in epoxy and polished. After preliminary examination in reflected light, the microscopic features of run products and phase compositions (Supplementary Table 2) were studied by means of BSE with a CamScan MV2300 (VEGA TS 5130MM) electron microscope equipped with the EDS electron microprobe Link INCA Energy. Some samples were examined twice or thrice after repeated polishing. Microprobe analyses of crystalline phases were performed at 20 kV accelerating potential, 10 nA of beam current and beam diameter of 3 μm. Microprobe analyses of glasses and the products of melt quenching were performed using a rastered beam over areas 500–20 $\mu m^2$. The quenched melt was assumed to be homogeneous if analyses from large areas (up to 500 $\mu m^2$) show composition similar to smaller areas (down to 20 $\mu m^2$). The following standards were used both for crystalline phases and quenched melts: synthetic $SiO_2$ for Si, synthetic MgO for Mg, synthetic $Al_2O_3$ for Al, natural wollastonite for Ca, and natural microcline and albite for K and Na, respectively, and synthetic NaCl for Cl. The ZAF matrix correction was used. No normalization procedure is applied. Compositions of the quenched melts and salt phases in the quenching products (Supplementary Table 2) are shown as weight percent of elements. This allows comparison of carbonate–silicate and chloride–carbonate liquids, since the oxygen basis for the chloride–carbonate liquids is not fully justified. No special attempt to analyze carbon in the quenched melts was made. All analyses of the quenched melts in Supplementary Table 2 show low total oxide content (below 95 wt.%). As assumed by some authors [50–53], the difference between the total oxide content and 100% roughly reflects a concentration of $CO_2$ in the quenched melts. Therefore, in our study we accept that this difference can be tentatively used as a marker for variation of carbonate component with respect to other components in the melts. This difference is positively correlated with the carbonate content in the starting mixtures.

Infrared absorption spectra for chloride–carbonate–silicate glasses from several run products were collected in reflection mode using Bruker IFS66 spectrometer equipped with IR microscope using an aperture of 100 μm. Spectra were recorded between 600 and 5000 $cm^{-1}$ at 4 $cm^{-1}$ resolution. The IR data were evaluated with the OPUS-5 software. We have measured relative intensities of bands at 1400 $cm^{-1}$ (representative for $CO_3^{2-}$ groups [54]) and 950 $cm^{-1}$ (representative for the Si–O–Si groups [54]) in these glasses and found the perfect negative correlation of the $I_{1400}/I_{950}$ parameter both with the silica content in the glasses and the difference between the total oxide content and 100%. These correlations supported the idea to use the above difference as a marker for the carbonate content in the melts.

## 3. Experimental results

In order to consider the phase relations of the complex chloride–carbonate–silicate melts in the system $CaMgSi_2O_6$–($CaCO_3$, $Na_2CO_3$)–KCl, we have to know phase relations in the boundary pseudo-binary joins (1) $CaMgSi_2O_6$–KCl, (2) $CaMgSi_2O_6$–($CaCO_3$, $Na_2CO_3$), and (3) ($CaCO_3$, $Na_2CO_3$)–KCl.

### 3.1. Join $CaMgSi_2O_6$–KCl

Experiments in this boundary join were performed at temperatures up to 1730 °C. Despite of clear evidence for melting of chloride (quenched aggregates of elongated KCl crystals), no detectable signs of interaction between the chloride melt and diopside were identified (Fig. 2a). Chloride quench shows up 0.15 wt.% of $SiO_2$ and 0.1–0.4 wt.% of CaO without MgO. Such composition of the quench, probably, reflects an insignificant incongruent dissolution of diopside in the KCl melt.

The observed phase relations up to 1730 °C imply that the T–X topology of the join is similar to the topology of a binary system with two immiscible liquids, where the liquidus temperature within the liquid immiscibility compositional interval is close to the melting temperature of the most refractive component (diopside). Below this temperature crystalline diopside coexists with the chloride melt, which slightly dissolves the silicate substance. Thus, we assume liquid miscibility gap in the join diopside–KCl at 5 GPa and above 1800 °C.

### 3.2. Join $CaMgSi_2O_6$–$Na_2CO_3$(±$CaCO_3$)

Liquid immiscibility in this join was observed at low pressure [41,42]. In the run #1/1232 (Supplementary Table 1), the quenched material shows an inhomogeneous texture that is expressed in ovoidal segregations of delicate dendrital quenching crystals cemented by homogeneous glass (Fig. 2b). Nevertheless, the compositional homogeneity of the quench was observed. Therefore, the quenched material is formed from the homogeneous carbonate–silicate melt. No crystalline phases were identified in the products from the same mixture at 1500 and 1400 °C (Supplementary Table 1), suggesting a low temperature liquidus of alkali-rich carbonate–silicate melts.

### 3.3. Join ($Na_2CO_3$, $CaCO_3$)–KCl

No data on phase equiliria in chloride–carbonate systems at high-pressure are available so far. No liquid immiscibility in the reciprocal systems including $CaCO_3$, $CaCl_2$, $Na_2CO_3$, NaCl, $K_2CO_3$, KCl is observed

at ambient pressure (see [55] and references therein). Thus, no liquid immiscibility should be expected at high pressures. Spectacular quenching textures in the run products at 5 GPa and 1500 °C (Fig. 2c) prove this conclusion. Homogeneity of the quenched material was verified with rastered microprobe analyses.

Thus, experiments in the boundary joins of the system $CaMgSi_2O_6$–($CaCO_3$, $Na_2CO_3$)–KCl at 5 GPa demonstrated that (1) melts both in the carbonate–silicate and chloride–carbonate joins are homogeneous liquids; (2) high-temperature liquid immiscibility is characteristic for the chloride–silicate join; (3) presence of pure chloride does not influence on melting temperatures of Ca–Mg silicates. Higher temperatures of melting in the chloride–silicate join with respect to the carbonate–silicate and chloride–carbonate joins assume that the carbonate-rich portion of the pseudo-ternary system is much of lower-temperature, and evolution of complex melts would proceed toward the carbonate apex during cooling.

### *3.4. Pseudo-ternary system $CaMgSi_2O_6$–($CaCO_3$, $Na_2CO_3$)–KCl*

#### *3.4.1. Textural relations in the run products*

Quenched melts were identified in all run products of the experiments in the ternary system (Fig. 3a–f). Two groups of the run samples are distinguished: (1) the run samples showing clear textural evidences for liquid immiscibility (Fig. 3a, c, d, e) and (2) the run samples containing homogeneous melt only (Fig. 3b, f). In addition to quenched melt, some run samples contain diopside and/or merwinite (Fig. 3b, e, f).

The specific feature of the first-group run samples is the globular textures (Fig. 3a, c, d, e). Both chloride–carbonate globes in the carbonate–silicate glass and carbonate–silicate glass globes in the chloride–carbonate matrix are identified in the run samples. In the most cases, the chloride–carbonate globes in carbonate–silicate glass are spherical or ellipsoidal. However, globes of irregular shape with rounded outlines are observed in the run sample #1/1236 (Fig. 3a). Diameter of the chloride–carbonate globes varies from several microns to 1000 μm (see Fig. 3d). In presence of diopside crystals, the globes are attached to them, but no diopside crystals are observed inside the globes. The globes are composed of finely grained aggregates of KCl intermixed with unidentified carbonates and silicates. In the relatively carbonate-poor globes (corresponding to the low-carbonate starting mixtures), KCl forms "brain-like" aggregates (Fig. 3e), where interstices between KCl grains is filled with carbonate–silicate material. In addition to KCl crystallites, the globes contain NaCl or (K, Na)Cl cubes. Locally, delicate glass balls are present in the globes. With increase of the carbonate content in the chloride–carbonate globes, the delicately interlaced sheaf-like aggregates of chloride grains and acicular carbonate crystals (see an inset in Fig. 3d) appear in the product texture. The texture ruled by carbonates becomes more distinct in the carbonate-rich globes (Fig. 3a). According to microprobe analyses, major carbonate phases in the globes are K–Ca varieties. In addition to spherical globes, chloride–carbonate aggregate forms shapeless layers and cumulates in the glass, which are mostly attached to upper zones of the capsules. They imply an upward floatation of chloride–carbonate material in the silicate melt during the runs. Glassy (carbonate–silicate) spherical and ellipsoidal globes of different sizes (from 0.5–1 μm to 10–20 μm) plunged into the chloride–carbonate matrix are characteristic for the run products of the experiments with the carbonate-rich mixtures (Fig. 3c, f). As a rule, large glassy globes contain numerous chloride–carbonate globes (Fig. 3c). Thus, rounded shapes of both chloride–carbonate and glassy globes and spectacular "globe-in-globe" textures in some samples unambiguously suggest a liquid immiscibility between carbonate–silicate and chloride–silicate melts under the experimental P–T conditions.

Some samples (Supplementary Table 1) contain neither chloride–carbonate nor glassy globes, while quenching textures represent a homogeneous melt (Fig. 3b, f). Diopside and merwinite form large crystals, associated both with carbonate–silicate glasses and the chloride–carbonate aggregates (Fig. 3b, e, f). If both merwinite and diopside are present in a run sample, aggregates of diopside grains replaces large merwinite subhedral crystals at their contact with the quenched melt (Fig. 3b) suggesting possible peritectic relations (Mrw + $L$ = Di) between these phases. Run products of the experiments #1516 (containing diopside only) and #1459 (containing both diopside and merwinite) indicate that this reaction, probably, proceeds to the right with decrease of temperature in the interval 1500–1400 °C (Supplementary Table 1).

Supplementary Table 1 indicates regular changes of phase relation in the run samples produced in a single starting mixture at different temperatures. For example, mixture $[\text{mix. } 1]_{87}Di_{13}$ produces merwinite coexisting with homogeneous chloride–carbonate melt at 1500 °C (run #1458). However, crystals disappear, while globular textures appear in the products at 1600 °C (Fig. 3c). Similar sequence is observed in the run products with the mixtures $[\text{mix. } 1]_{71}Di_{29}$, $[\text{mix. } 1]_{56}Di_{44}$, and $[\text{mix. } 3]_{50}Di_{50}$ within the interval 1400–1600 °C (Supplementary

Table 1). Thus, dissolution of crystalline silicates in the chloride–carbonate liquid and its saturation with silica results in splitting of the homogeneous melt into chloride–carbonate and carbonate–silicate immiscible melts.

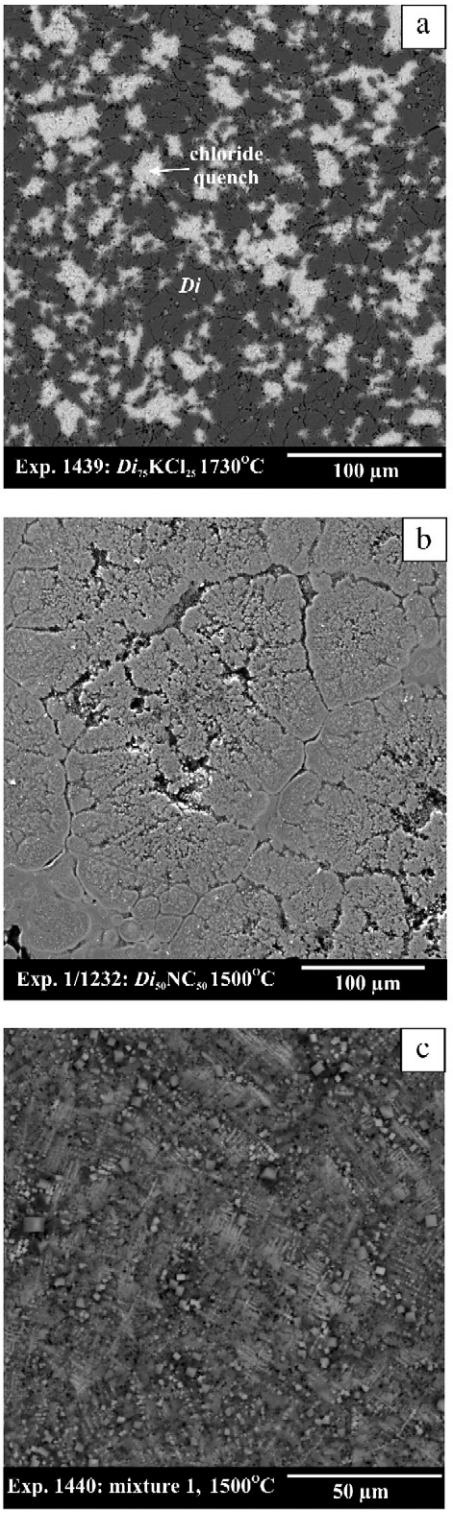


Fig. 2. Textural relations in the run samples representing the boundary joins of the system $CaMgSi_2O_6$–($CaCO_3$, $Na_2CO_3$)–KCl at 5 GPa. (a) No reaction between diopside crystals and the KCl melt in the join $CaMgSi_2O_6$–KCl; (b) Specific ovoidal textures formed during quenching of the homogeneous carbonate–silicate melt in the join $CaMgSi_2O_6$–$Na_2CO_3$; (c) Spectacular dendrital textures resulted from the quenching of the homogeneous chloride–carbonate liquid in the join ($CaCO_3$, $Na_2CO_3$)–KCl. All images are taken with CamScan MV2300 (VEGA TS 5130MM) microscope.

In addition, Supplementary Table 1 shows that addition of 44 wt.% of diopside into the chloride–carbonate mixture (mix. 1) results in splitting of the initially homogeneous chloride–carbonate melt (Fig. 2c) into chloride–carbonate and carbonate–silicate immiscible liquids at 1500 °C (Fig. 3d). In turn, 29 wt.% of KCl added in the carbonate–silicate mix. 5 (Supplementary Table 1) causes immiscibility, as well. Thus, the addition of silicate components into the chloride–carbonate melts and chloride components into the carbonate–silicate melts leads to the formation of the immiscible chloride–carbonate and carbonate–silicate liquids.

### *3.4.2. Melt composition in the run products*

Three compositional groups of melts are distinguished in the run products: (1) homogeneous chloride–carbonate–silicate melts; (2) chlorine-bearing carbonate–silicate melts, that are immiscible with (3) the silica-poor chloride–carbonate melts.

As a rule, homogeneous chloride–carbonate–silicate melts coexist with diopside and/or merwinite (Supplementary Table 1; Fig. 3b). Concentration of Si in these melts positively correlates with the difference [100 — oxide total] (Fig. 4). This correlation implies that the saturation limit of chloride–carbonate melt with silica increases with increase of the carbonate content in them. The carbonate content in the homogeneous melts, coexisting with crystalline silicates, increases with decrease of temperature (Fig. 4).

Compositions of the carbonate–silicate melts coexisting with immiscible chloride–carbonate liquids are mostly determined by the bulk composition of the starting mixture (Fig. 5a–g). Concentration of Si varies within the range of 10–19 wt.% and negatively correlates with the difference [100 — total oxide] (Fig. 5a). The observed negative correlation corresponds to isomorphism $SiO_2 \Leftrightarrow CO_2$ in the carbonate–silicate melts. The diagram shows that at constant Si, the difference [100 — total oxide] decreases with increase of temperature, i.e. low-temperature melts are, presumably, more carbonatitic. The Si content in the melts positively correlates with Mg,

reflecting variation of the diopside component in the starting mixtures (Fig. 5b). However, Fig. 5b indicates positive correlation between Mg concentration in the melts and temperature at constant Si.

All melts are highly calcic (10–23 wt.% Ca) and alkalic (10–24 wt.% of K+Na) reflecting high calcium and alkali contents in the starting mixtures. Nevertheless, the K/Na ratio in the carbonate–silicate melts

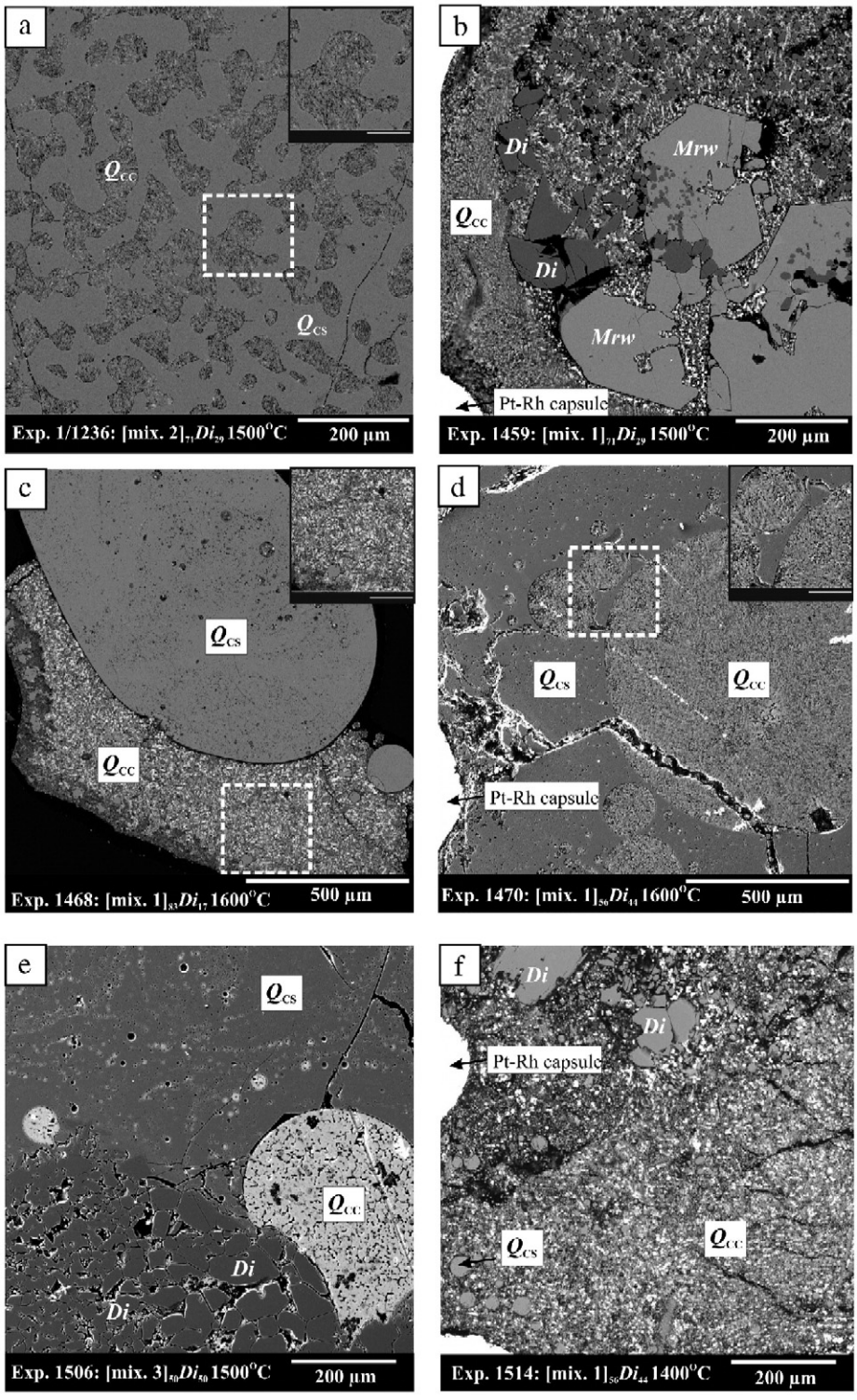

that were produced from starting mixtures of similar bulk composition regularly increases with increasing temperature for relatively silica-rich melts, while decreases for carbonate-rich melts (Fig. 5c). The regular variation of the K/Na ratio in the melts coexisting with KCl-rich immiscible liquids implies that solubility of K and Cl is regulated by complex exchange reactions with silicate and carbonate components in the melts, rather than simple solubility of KCl. Such exchange reaction should inevitably result in separation of K and Cl in the carbonate-silicate melts. This conclusion is supported by an increase of the K/Cl ratio with the Si content in the melts (Fig. 5d), while this ratio (in wt.%) in all melts is >1.1 (corresponding to this ratio in pure KCl). Thus, the higher silica in the melts the higher potassium content and lower chlorine in them at constant T and P.

Chlorine content in the carbonate–silicate melt equilibrated with KCl-rich chloride–carbonate liquid reaches 4–5 wt.%, while it distinctly decreases down to 1–2 wt.% in Si-rich melts (Fig. 5e). Moreover, chlorine concentration in the carbonate-rich melts decreases by 1–2 wt.% with increasing temperature. Chlorine content in the Si-rich melts is approximately the same at temperatures 1500 °C and 1600 °C (Fig. 5e). Decrease of the Cl content in melts is not related to the bulk composition of starting materials, but is strongly determined by the silica content in corresponding melts. The negative correlation between Si and Cl content is well known for silicate melts of wide-range compositions at low pressures (e.g. [13,14] and references therein). Data by Suk [41,42] show similar negative correlation between Si and Cl in the carbonate–silicate melt in its equilibrium with chloride–carbonate liquid at 0.2 GPa. Our experimental results for the mixture Di–$Na_2CO_3$–KCl at 5 GPa and 1500 °C (run #1508 in Supplementary Table 1) can be compared with Suk's data (2001, 2004) for the mixture Di–$Na_2CO_3$–NaCl at 0.2 GPa and 1110 °C. At the comparable $SiO_2$ contents (about 40 wt.%), melts from the run #1508 contain about of 2.5 wt.% of chlorine, while the Cl concentration in Suk's [48,49] run products is just about 1.2 wt.%. It would be prettily concluded that the Cl content in the melts is a function of pressure. However, in our case, it is hard to make a final decision, since our runs and runs by Suk [41,42] were conducted at incomparably different temperatures. In general, Cl content increases from silica-rich toward the carbonate-rich melts, so far (Fig. 5a and e).

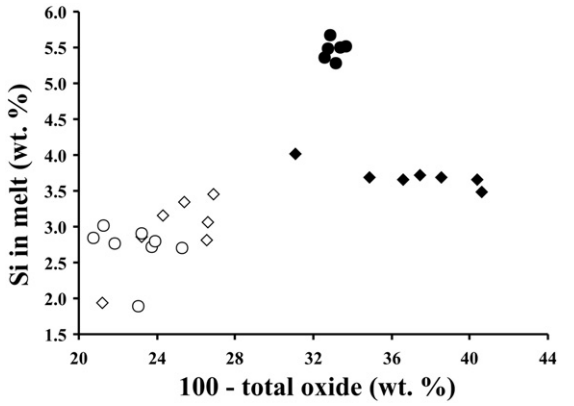


Fig. 4. Dependence of Si content in homogeneous chloride–carbonate–silicate melts coexisting with diopside and/or merwinite on the difference [100 — total oxide], reflecting the content of the carbonate component. Open symbols correspond to melts at 1500 °C (diamonds — exp. 1458, circles — exp. 1459), while filled symbols indicate melts at 1400 °C (diamonds — exp. 1516, circles — exp. 1517).

The chlorine content in the carbonate–silicate melts at 5 GPa shows no distinct correlation with the Ca content. Thus, Ca is not the factor regulating chlorine solubility in the melts. No any apparent correlation between Cl and Na is observed for most of synthetic melts (Fig. 5f). Sodium, therefore, is not a strong promoter of Cl solubility, as well. In general, Cl increases with K in the melts (Fig. 5g). There are two distinct groups of data points in Fig. 5g, each of which shows positive correlation of K and Cl. The high-potassium group of the data points includes melts of the runs #1501 and #1506, performed from the Si-rich starting mixture $[\text{mix. 3}]_{50}Di_{50}$ (Supplementary Table 1), and melt of the run #1508, that is produced from the $Na_2CO_3$-rich starting mixture $[\text{mix. 5}]_{71}KCl_{29}$ (Supplementary Table 1). These relations show that along with high Si content (Fig. 5d), the displacement of the equilibrium $Na_2CO_3$ ($L_{CS}$)+KCl ($L_{CC}$)=$K_2CO_3$($L_{CS}$) +NaCl ($L_{CC}$) to the right could be an effective mechanism for enrichment in potassium of the carbonate–silicate melts without significant enrichment in chlorine in

Fig. 3. Textural relations in the run samples representing the pseudo-ternary system $CaMgSi_2O_6$–($CaCO_3$, $Na_2CO_3$)–KCl at 5 GPa. (a) Irregularly shaped chloride–carbonate globes with rounded outlines in the carbonate–silicate glass; the inset (scale bar is 50 μm) demonstrates the sheaf-like texture of the acicular chloride–carbonate aggregate in the globes. (b) Large euhedral crystals of merwinite partially replaced by the aggregates of diopside grains in the quenching products of homogeneous chloride–carbonate melt. (c) and (d) Clear immiscibility between chloride–carbonate and carbonate–silicate melts; textures "globe-in-globe" are evident in the image (c): carbonate–silicate glass contains numerous chloride–carbonate globes, whereas the chloride–carbonate quench is crowded with glassy globes; the inset in the image (c) (scale bar is 50 μm) illustrates the texture of the chloride–carbonate quench with rounded glassy globes; the inset in figure (d) (scale bar is 50 μm) demonstrates in detail the texture of the chloride–carbonate globes in the carbonate–silicate glass. (e) and (f) Coexistence of the immiscible liquids with diopside at 1500 and 1400 °C. All images are taken with CamScan MV2300 (VEGA TS 5130MM) microscope.

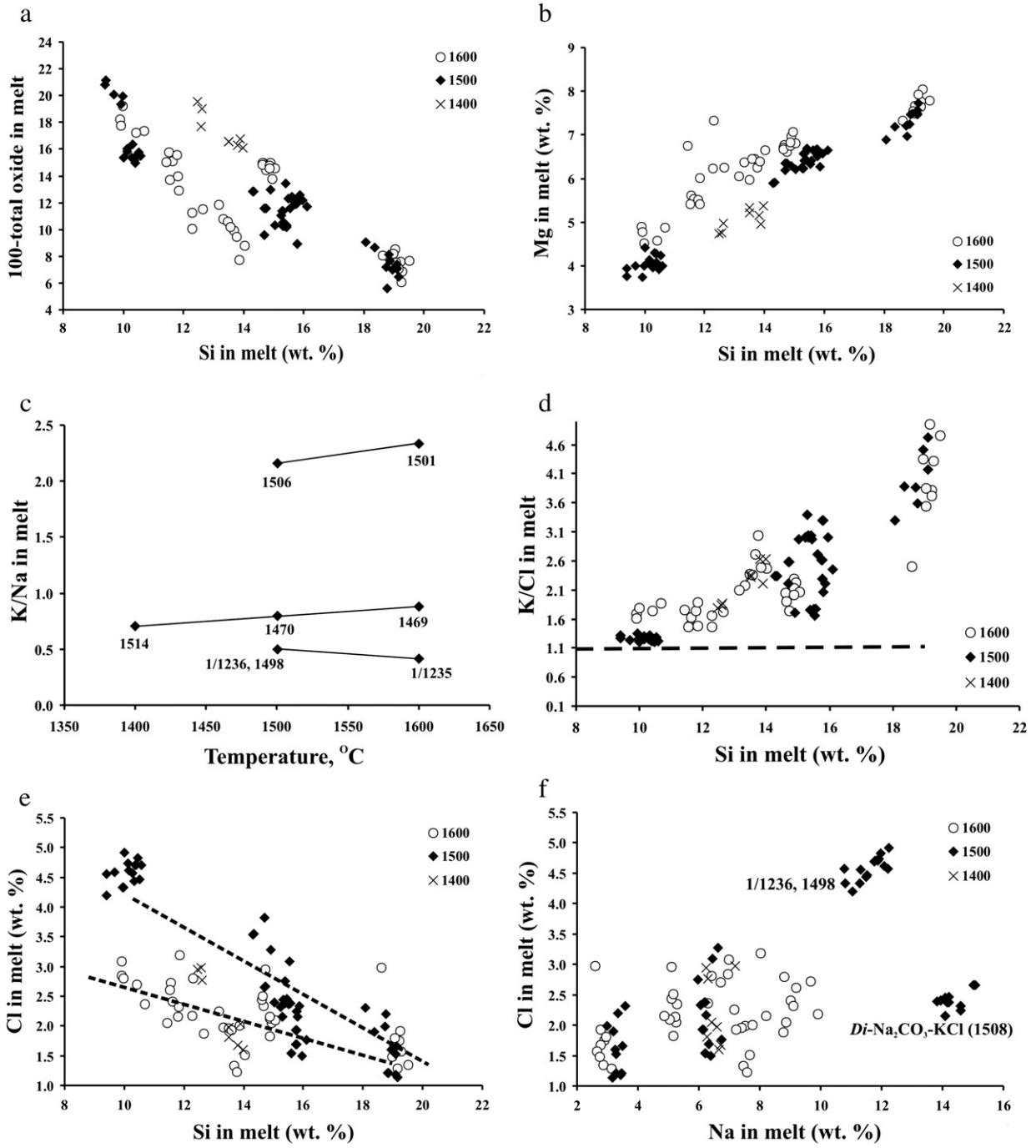


Fig. 5. Specific compositional features of the carbonate–silicate melts, coexisting with immiscible chloride–carbonate liquids. (a) Dependence of the difference [100 — total oxide] on the Si content, reflecting the possible isomorphism $SiO_2 \Leftrightarrow CO_2$ in the melts. (b) Positive correlation of the Mg and Si contents in the melts indicating also the dependence of the Mg concentration on temperature. (c) Variations of the K/Na ratio on temperature for the melts produced in the silicate-rich mixture [mix. 3]$_{50}$Di$_{50}$ (runs 1506 and 1501), mixture [mix. 1]$_{56}$Di$_{44}$ (runs 1514, 1470, and 1469), and carbonate-rich mixture [mix. 2]$_{71}$Di$_{29}$ (runs 1/1236, 1498, and 1/1235). (d) Increase of the K/Cl ratio in the melts with the Si content (dashed line indicates the K/Cl ~1.1 corresponding to pure KCl). (e) Negative correlation of the Cl content with the Si concentration in the melts. (f) Dependence of the Cl content on the Na concentration in the melts (the experiments 1508, 1/1236, and 1498 are labeled for comparison discussed in the text). (g) Positive correlation of the Cl content with the K content in the melts.

equilibrium with the immiscible chloride–carbonate liquid. This mechanism is supported by high concentration of Na (up to 16 wt.%) in the chloride–carbonate globes from the run products (Supplementary Table 2). General variations of composition of the chloride–carbonate melts will be discussed below.

### 3.4.3. Phase relations in the chloride–carbonate–silicate system

Liquid miscibility gaps are constructed from the compositions of the coexisting carbonate–silicate melt and chloride–carbonate brine in the ternary system $CaMgSi_2O_6$–($CaCO_3$, $Na_2CO_3$)–KCl (Fig. 6a–c). Branches of the miscibility gaps converge at the (Ca+Mg+Na) apex of the triangular diagram (point *k*), which corresponds to the carbonate–rich compositions (Fig. 6a–c). For the carbonate-rich compositions, the tie-lines have gentle slopes. The chloride-rich ends of the tie-lines migrate toward the KCl apex with decreasing carbonate content, and for the silicate-rich composition $[\text{mix. 3}]_{50}Di_{50}$ (Supplementary Table 1) they are situated immediately at this apex. Probably, these relations correspond to preferential partitioning of the carbonates to the carbonate–silicate melt rather than in the chloride–carbonate brine.

Fig. 6a–c allows the tracing of the major changes in phase relations in the complex chloride–carbonate–silicate system with temperature at pressure 5 GPa. Crystalline phases are absent in the run products at 1600 °C,

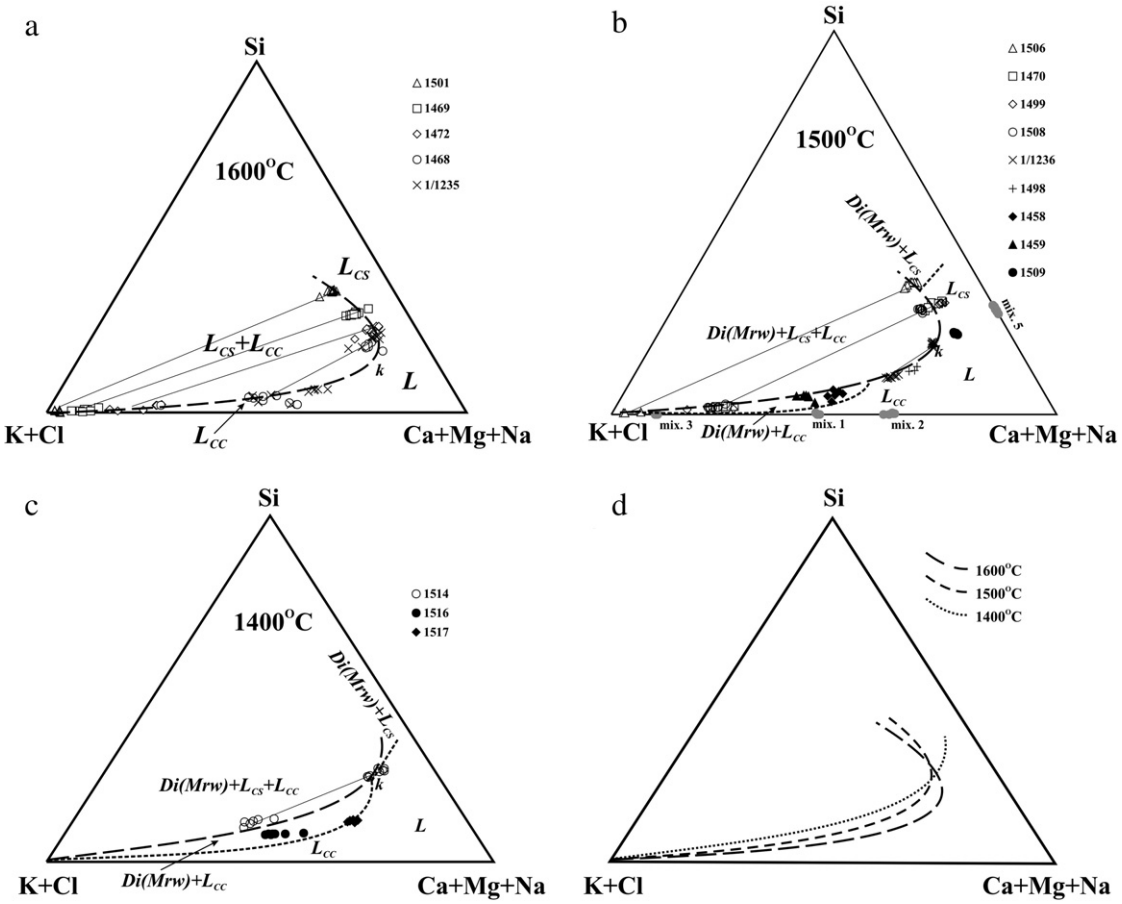


Fig. 6. Schemes illustrating evolution of phase assemblages and shape of the miscibility gap in the carbonate-rich portion of the ternary system $CaMgSi_2O_6$–($CaCO_3$, $Na_2CO_3$)–KCl at 5 GPa. (a) 1600 °C. No crystalline phases are observed, while the miscibility gap is expended toward the (Ca+Mg+Na) apex. (b) 1500 °C. Diopside and/or merwinite appear with the immiscible liquids, while the field of the homogeneous melt (*L*) slightly expends; (c) 1400 °C. Phase fields Di(Mrw)+$L_{CC}$, Di+$L_{CS}$, and the field of the homogeneous melt (*L*) are greatly expended at expanse of the miscibility gap. (c) Rough comparison of miscibility gaps at 1600, 1500, and 1400 °C, constructed in the diagrams a, b, and c. Liquids within the miscibility gap: $L_{CS}$ — carbonate–silicate liquid and $L_{CC}$ — chloride–carbonate liquid; *L* — homogeneous liquid. Long-dashed lines schematically mark boundaries of the miscibility gap, while thin lines are tie-lines connecting compositions of the coexisting liquids. Short-dashed lines schematically indicate boundaries of pseudo-liquidus fields Di(Mrw)+$L_{CC}$ and Di+$L_{CS}$.

while clear evidences for the liquid immiscibility are present (Supplementary Table 1; Fig. 3c, d). The convergence point (*k*) is located close to the (Ca+Mg+Na) apex, whereas the phase fields *L* and $L_{CC}$ are narrow (Fig. 6a). The phase relations drastically change at 1500 °C (Fig. 6b). Diopside and merwinite (Fig. 3b, e, f) manifest an appearance of phase fields Di(Mrw)+$L_{CC}$, Di(Mrw)+$L_{CS}$, and Di(Mrw)+$L_{CS}$+$L_{CC}$ (we do not separate Di and Mrw in the schematic diagram, since no specific experiments were performed to study their peritectic relations). However, these phase fields do not extend to the carbonate portion of the diagram. The convergence point (*k*) moves slightly further from the (Ca+Mg+Na) apex (Fig. 6b). In turn, the phase fields *L* and $L_{CC}$ become wider at the expense of the miscibility gap (Fig. 6b). The subsequent drop of temperature down to 1400 °C results in further displacement of the convergence point from the (Ca+Mg+Na) apex and widening of the phase fields *L*, Di(Mrw)+$L_{CC}$, Di(Mrw)+$L_{CS}$, and $L_{CC}$. The liquidus assemblages Di(Mrw)+$L_{CC}$ and Di(Mrw)+$L_{CS}$ spread further to the carbonate-rich portion of the system toward the (Ca+Mg+Na) apex (Fig. 6c). Probably, these fields meet each other in the convergence point (*k*), resulting in a minimum on the miscibility gap. Comparison of the above miscibility gaps at 1600, 1500, and 1400 °C (Fig. 6d) indicates general modifications of the phase relations with decreasing temperature: (1) the miscibility gap displaces toward the more silica-rich portion of the system and (2) the compositional ranges for the homogeneous silica-bearing chloride–carbonate brine significantly widens.

In order to explain the observed temperature variation in the shape and position of the miscibility gap, we consider the evolution of phase equilibria for bulk compositions [mix. 1]$_{71}$Di$_{29}$ and [mix. 1]$_{56}$Di$_{44}$ (Fig. 7a, b). In products of runs #1472 and #1467 (Supplementary Table 1) formed from the first mixture at 1600 °C, two melts coexist, while crystalline phases are absent. At 1500 °C, both diopside and merwinite crystallize and coexist with chloride–carbonate homogeneous melt. The composition of the melt displaces both toward the (Ca+Mg+Na) apex and becomes enriched is Si, as well. This process is reflected in reaction $L_{CC}^{(1)}+L_{CS}^{(1)}\rightarrow$Di(±Mrw)+$L_{CC}^{(2)}$ (Fig. 7a). Precipitating silicates remove Si from the melt, assisting, thereby, miscibility of chloride–carbonate and carbonate–silicate liquids. Subsequent cooling down to 1400 °C gradually destroys merwinite via reaction Mrw+$L_{CC}^{(2)}\rightarrow L_{CC}^{(3)}$(±Di), enriching further the melt with Ca, Mg, and Si. As the result, over temperature 1600–1400 °C the bulk composition of the chloride–carbonate liquid strongly displaces toward the carbonate-rich portion of the system, becoming simultaneously enriched in Si.

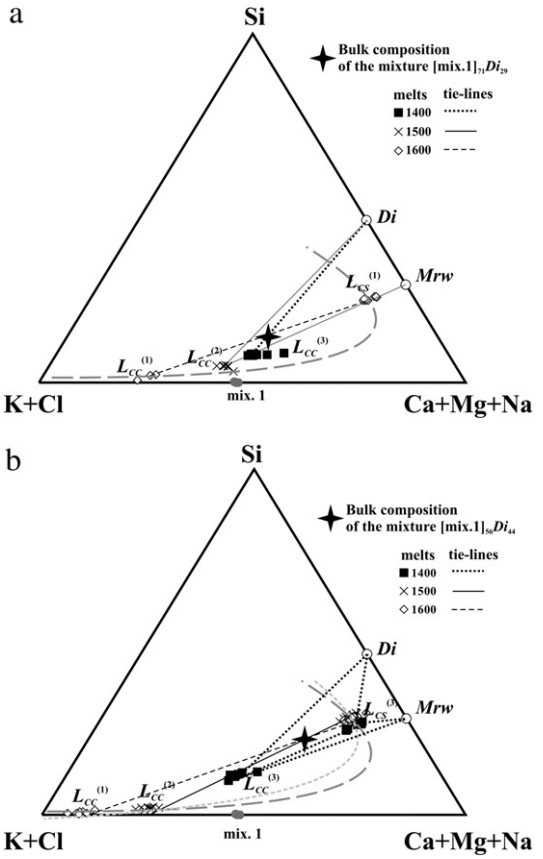


Fig. 7. Evolution of the phase relations and melt compositions with temperature in the system corresponding to the starting mixtures (a) [mix. 1]$_{71}$*Di*$_{29}$ and (b) [mix. 1]$_{56}$Di$_{44}$ (see Section 3.4.3 for discussion). Grey dashed line shows the miscibility gaps at 1600 °C (long-dashed) and 1500 °C (short-dashed) (see Fig. 6b).

At all temperatures, run products in the second mixture [mix. 1]$_{56}$Di$_{44}$ contain clear evidences for liquid immiscibility (Fig. 3d). Decreases of temperature from 1600 ($L_{CC}^{(1)}$) to 1500 °C ($L_{CC}^{(2)}$) drives composition of the chloride–carbonate melt toward the carbonate-rich portion of the system (Fig. 7b). The carbonate–silicate melt slightly depletes in Ca and Mg. However, at 1400 °C, the chloride–carbonate melt strongly accumulates Si, Ca, Mg, and Na, while the carbonate–silicate melt looses Si (Fig. 7b). Rapprochement of the melt compositions ($L_{CS}^{(3)}$ and $L_{CC}^{(3)}$) can be easily explained by precipitation of Di and Mrw, who extracts Si from the carbonate–silicate melt. As a result, the carbonate–silicate melt actively dissolves in the coexisting chloride–carbonate brine. Since the composition $L_{CS}^{(3)}$ is situated inside the triangle $L_{CC}^{(3)}$–Di–Mrw (Fig. 7b), we assume that the carbonate–silicate melt may disappear at temperature below 1400 °C due to reaction $L_{CS}^{(3)}\rightarrow L_{CC}^{(3)}$+Di+Mrw. Thus, precipitation of silicates from the melt is a major factor resulting in the

formation of homogeneous Si-saturated chloride–carbonate melt at lower temperatures.

## 4. Discussion and application to the mantle alkalic liquids

Navon and co-authors [22,24,37] explain transitions between silicate and carbonate melts preserved as inclusions in diamonds (Fig. 1) by two major mechanisms: (1) partial melting of carbonate-bearing mantle rocks or (2) fractional crystallization of initial liquid (probably, kimberlite-like). The first mechanism is based on the fact that carbonated peridotite yields a dolomitic partial melt at depths 70–200 km ([56] and references therein). With increasing degree of melting, the carbonaitic melts become richer in $SiO_2$ approaching to the composition of kimberlitic melts [50,51,57]. Similar regularities in evolution of the melt composition are observed in melting of carbonated eclogites, as well [58]. Thus, partial melting can explain the evolution of the liquids from carbonate-rich to carbonate–silicate [50,51,57,58]. The carbonate–silicate melts are able to intensively dissolve supercritical aqueous fluids saturated with alkalis and silica [56,59] continuing the trend toward the silica-rich liquids. Fractional crystallization implies that the crystallization of carbonates would displace the melt composition to more silica-rich varieties. Geochemical similarities between trapped liquids in diamonds and host kimberlites suggest origin of the melts from a kimberlitic magma [24,60].

However, the above models unable explain the formation of chloride–carbonate brines. Brine can be produced only by unusually intensive fractional crystallization, which drives the chlorine content from about of 3 up to 40 wt.% [37]. Melting of chlorine-depleted mantle rocks is not a mechanism for the formation of those brines, as well. Thus, the potassic chloride–carbonate brines may exist in the upper mantle as an independent liquid phase. High concentration of Cl in carbonate–silicate and carbonate inclusions in diamonds, on the one hand, and the continuous trends between chloride–carbonate and carbonate liquids (Fig. 1), on the other, implies that the brine, being independent, is closely associated with other constituents of alkali and chlorine-rich inclusions in diamonds.

Our present experiments unambiguously substantiated the liquid immiscibility model for the alkalic chloride–carbonate–silicate liquids in the upper mantle [37–39]. Of cause, direct comparison of compositions of the inclusions in diamonds with composition of the synthetic liquids is not fully justified, since natural liquids are much more complex in composition. For example, high concentrations of Ca and Na in the synthetic melts would be the factor, which is responsible for the overall higher chlorine content in these melts [13,14]. In contrast to the natural melts, the synthetic melts are undersaturated with water and do not contain such important components as Ti and P, which severely lower the chlorine content [13,14]. Temperatures of our experiments (1400–1600 °C) are much higher than temperatures estimated for the melt inclusions in diamonds [32,33]. Nevertheless, major compositional trends observed in the inclusions are identical to that of the synthetic melts. They include the following characteristics.

(1) Positive correlation of Cl with K (Fig. 5g) and negative correlation with Si (Fig. 5e, f; see also [22,24,27,29,30,32]).
(2) Increase of Si with the increase of the carbonate content is evident both for chloride–carbonate brine inclusions in diamonds [29,30,32] and the synthetic chloride–carbonate melts (see Fig. 6a–c).
(3) The ratio K/Cl>1 is characteristic both for natural and synthetic melts (Fig. 5d). K–Ca-carbonates in the chloride–carbonate globes reflect intensive exchange of components between KCl and carbonates. K-bearing carbonates are detected inside the chloride–carbonate inclusions in the Diavik diamonds [30].
(4) Positive correlation of the K/Cl ratio with the Si content in the synthetic carbonate–silicate melts (Fig. 5d) reflects bonding K with Si in the silica-rich varieties. Evidence for this bonding in natural assemblages is association of the carbonate–silicate melt inclusions with unique Si-rich mica [26,30,33].

Our experimental results demonstrate regular temperature trends for the immiscible carbonate–silicate and chloride–carbonate liquids. The data show that decrease in temperature results in evolution of both the Cl-bearing carbonate–silicate melt and the Si-bearing chloride–carbonate brine toward the low-temperature Cl-bearing carbonatitic liquid. Composition of the carbonate–silicate melt inclusions in some Botswanian diamonds varies from relatively $SiO_2$-rich to $SiO_2$-depleted and CaO-enriched liquids [22]. Chlorine is negatively correlated with silica. According to the data on variations of trace elements of sub-microscopic inclusions in Zairean diamonds [60], the major path for carbonate–silicate melts evolution proceeds from relatively silica-rich liquids toward the carbonate-rich ones. Shiryaev et al. [27] observed zoning of diamond BR-5 from Brazil (Fig. 1): inner zone is enriched in water and silicates, while the outer zone is carbonatitic with high concentration of Cl. These data are consistent with the temperature trend

constructed from the experimental data. They reflect diamond growth under decreasing temperature.

No evolution trends are reported for chloride–carbonate brine inclusions in diamonds from the Koffiefontein pipe [32,33], although carbonate-rich inclusions with high Cl content were reported in some of them [26]. Klein-BenDavid et al. [30] described the melt inclusions in three diamonds from the Diavik mine (Canada). The diamond ON-DVK-272 contains inclusions of chloride–carbonate potassium-rich brine, while the diamond ON-DVK-281 bears inclusions of the silica-poor carbonate–silicate melts (Fig. 1). The third diamond (ON-DVK-294) is zoned with respect to distribution of the melt inclusions [29,30]. Composition of inclusions in the inner zone is intermediate between the chloride–carbonate brine and carbonatitic liquid, while the outer zone contains essentially carbonatitic inclusions (Fig. 1). The brines in diamond ON-DVK-272 and in the inner zone of the diamond ON-DVK-294 form a single trend with the carbonatitic melt in the outer zone of the diamond ON-DVK-294. This apparent trend well agrees with the temperature trends constructed on the basis of our experimental data for the chloride–carbonate liquids. The average composition of melt inclusions in the diamond ON-DVK-281 is projected onto the silicate–carbonate join of the miscibility gap (Fig. 1). Thus, this diamond could grow from the carbonate–silicate melt that was immiscible with the chloride–carbonate brines preserved in other diamonds. Taking into account slopes of the tie-lines in Fig. 6a–c, this melt was, presumably, equilibrated with the high-temperature brine, preserved in the diamond ON-DVK-272. Melts in the diamond ON-DVK-294, probably, did not coexist with the immiscible liquids. Displacement of the miscibility gap boundaries toward the silica-rich field with decreasing temperature (Fig. 6a–c) allows evolution of the melts in the diamond ON-DVK-294 as low-temperature homogeneous liquids.

Interruptions in melt composition are recorded in zoning of diamond BR-5 [27] and diamond ON-DVK-294 [29,30]. Nevertheless, Klein-BenDavid et al. [29,30] mentioned that some intermediate inclusions were found between the inner (brine) zone and the outer (carbonatite) zone. Thus, the evolution of the liquids between two zones was interrelated. In our interpretation, the paucity in the diamond growth was, probably, related to change in temperature regime in the system, i.e. cooling. In turn, the cooling could be caused by "shutting-off" or weakening of an external thermal source. Cooling could result in change of isotopic composition [27,29].

On the basis of experimental results, we can consider the potassic Cl-rich carbonatitic liquids trapped in diamonds from the Yubileinaya [28,30], Diavik [29,30], and Koffiefontein [26] pipes as the most low-temperature liquids. This conclusion contradicts to the model of fractional crystallization proposed by Navon and his co-authors [22,24,37]. The key aspect of this model is a primary crystallization of carbonates, which drives compositions of carbonatitic liquids toward the silica-rich varieties. Our experiments indicate that liquidus phases in the Cl-saturated carbonate–silicate and the Si-saturated chloride–carbonate melts are silicates (Fig. 6a–c). Data on Cl-rich system are consistent with the experimental data on the Cl-free alkalic carbonate–silicate systems, which also clearly indicate that the carbonate–silicate melts precipitate silicate phases at liquidus [44,61]. Our results also consistent with the experiments on partial melting of carbonated mantle rocks [50,51,57,58]. Melts forming from the carbonated peridotites and eclogites vary from essentially carbonatitic to Si-saturated carbonate–silicate melts with increasing degree of melting, since carbonate–silicate systems at high pressures show perfect miscibility of the liquid end-member components. With addition of chlorides, this behavior is violated because of the immiscibility phenomena. In this case, the system would have a topology of a pseudo-binary T–X section penetrating the ternary system chloride–carbonate–silicate along an arbitrary (silicate+carbonate)–(chloride +carbonate) join (Fig. 8). Alkali-rich chloride–carbonate–silicate system begins to melt with the formation of carbonate-rich liquid saturated with both the chloride and silicate components (point *E* in Fig. 8). Subsequent evolution of the system would be determined by solubility of silicate component in the chloride–carbonate melt. Solubility of silicates is a complex function of temperature and carbonate content in the melt, which is impossible to depict in the schematic T–X section. However, there is a limit for saturation of the melt with the silicate compound for every bulk composition (a–b in Fig. 8). Above this limit, two immiscible liquids appear in the system.

Thus, the formation of carbonate–silicate Cl-bearing melts proceeds via liquid immiscibility with the silica-saturated chloride–carbonate liquids migrating through the silicate rocks. This model is supported by the direct observations of Si-bearing chloride–carbonate liquids in single inclusions together with garnets, pyroxenes, chromites, olivines [26,30,33]. Complex daughter crystals inside the inclusions and findings of unique silicate phases (e.g., high-Si mica) associated with inclusions are indubitable evidences for the interaction (equilibration) of the liquids with mantle minerals [26,30,33]. Safonov et al. [62] reported the formation of similar Si-enriched mica in the chloride-bearing system at 4 GPa. In our present experiments, we also observed reaction between

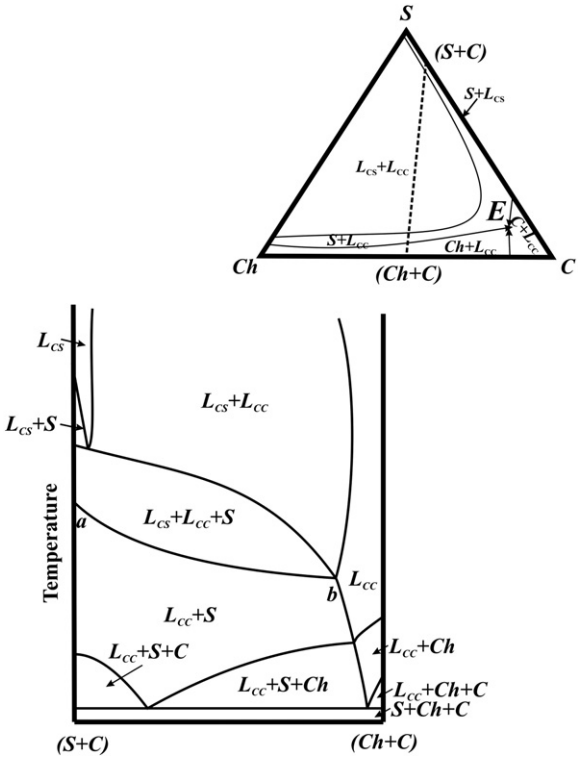


Fig. 8. Schematic T–X section of the pseudo-ternary system chloride–carbonate–silicate with the wide miscibility gap (see the inset picture) along an arbitrary join (silicate+carbonate)–(chloride+carbonate) (dashed line) at constant pressure. *S* — silicate, *C* — carbonate, *Ch* — chloride.

diopside and chloride–carbonate liquid with the formation of merwinite. Appearance of this silica-deficient phase is related both to low silica and high Ca contents in the coexisting melt. In the Mg-rich system we could expect formation of forsterite. The progress of reactions of the chloride–carbonate liquids with diverse minerals in complex natural rocks would explain diversity of alkaline chlorine-rich liquids preserved in diamonds. Liquid immiscibility in the chloride–carbonate–silicate melts greatly widens this diversity, since immiscibility results in abrupt change of the liquid composition. Appearance of two immiscible liquids would influence on the relative mobility of these liquids in the solid-dominated media (e.g. [63]). The predominant carbonate–silicate melt wetting the grain boundaries would be more mobile in contrast to the carbonate–chloride brine, which forms globes.

Our experiments do not involve water, which is an important constituent of the melt and brine inclusions in diamonds [21,22,27,29,30,32]. Presence of water could assist to miscibility of the liquids, expanding the compositional region of the homogeneous chloride–carbonate–silicate melt. Moreover, perfect solubility silicates in supercritical aqueous fluids (e.g. [56] and references therein) would result in further contraction of the miscibility gap. In the case of liquid immiscibility, water seems to preferentially partitions from the silicate-rich melt to the coexisting chloride–carbonate liquid, which serves as a dryer for the melt. This suggestion is supported by aqueous composition of the brine inclusions in diamonds (30–40 wt.% of water, [32]) in comparison with the carbonate–silicate inclusions, as well as extreme dryness of the Udachnaya–East kimberlite enclosing chloride–carbonate segregations [12].

High Si/Mg ratio, high Ca and alkali contents of the synthetic melts are different from kimberlite. Nevertheless, our experiments give some general implications for a model of the formation of Cl-enriched kimberlites of the Udachnaya–East pipe [10–12]. Kamenetsky et al. [12] estimated chlorine content above 7 wt.% in the chloride–carbonate–silicate magma producing these unique kimberlites. Taking into account compositions of the kimberlite groundmass and the chloride–carbonate liquid preserved as inclusions in olivine [12], we can roughly estimate that the primary magma could contain up to 40 wt.% of the alkali chloride–carbonate component. It corresponds to about 22 wt.% of $SiO_2$ (or about 10 wt.% of Si). Our experiments show that such magma is hardly to be homogeneous at 5 GPa. We assume that kimberlitic magma already coexisted with the chloride–carbonate immiscible liquid during its formation. The chlorine content about of 2.5 wt.% in the kimberlite groundmass is consistent with the chlorine concentration in the synthetic melts (Fig. 5e). However this conclusion is true for temperatures 1400–1600 °C, while at T ~1000 °C [12] coexistence of a homogeneous melt with abundant solid phases is quite possible. But, in this case, it could be Cl-rich carbonatitic magma rather than kimberlitic one. Thus, the model for the formation of the Cl-rich kimberlite would include progressive melting and splitting into two melts, kimberlitic and chloride–carbonate. In contrast to the formation of "usual" kimberlitic melts, these processes could occur at relatively low temperature owing to the presence of the alkalic chloride–carbonate liquids.

## 5. Conclusion

Presented experimental data unambiguously indicate that the liquid immiscibility as a major mechanism controlling evolution and diversity of the alkalic Cl-rich liquids in the upper mantle. However, it is hard to state that these liquids are ubiquitous in the mantle. More likely, that the above processes are localized and occur

at low degrees of partial melting of the mantle rocks. This is supported by high enrichment of the chlorine-rich liquids in trace elements, chlorine, phosphorus, and alkalis with complimentary depletion in Al and Cr. Nevertheless, the liquids precipitate diamonds [64–69] and, probably, are able to trigger much more voluminous processes, like kimberlitic magmatism. Geochemical and isotopic data show close relation of the carbonate–silicate and carbonatitic melt inclusions in fibrous diamonds with basaltic kimberlites (group I) [24,60,70]. Our experiments indicate that these melts could form as immiscible phase during interaction of chloride–carbonate liquids with the mantle rocks. It brings forth a problem of participation of the chloride–carbonate liquids in the kimberlite genesis. Moreover, most the petrological data on chlorine activity in the upper mantle, briefly summarized in the introduction, came from kimberlites.

## Aknowledgments

Fruitful discussions with Oded Navon, Alexander Sobolev, Vadim Kamenetsky, Andrey Shiryaev gave new ideas in the present study. We thank Oded Navon for some unpublished data on compositions of the melt inclusions in diamonds from India and Yakutia. The authors are very grateful to Ludmila P. Red'kina for preparation of starting materials and mixtures. Nikolai Boldyrev provided facilities for the IR study of the run products, while Andrey Shiryaev helped to evaluate the obtained IR spectra of glasses. We thank Alexei Nekrasov and Konstantin Van for providing facilities for electron microprobe analyses. The study is supported by the Russian Foundation for Basic Research (projects #04-05-64896 to OGS, #06-05-64196 to LLP, #05-05-64101 to YAL), the RF President's Grant for Young Scientists (Project #MK-969.2006.5 to OGS), the RF President's Leading Scientific Schools Program (grant #5338.2006.5 to LLP), the RAS Project #P-9-3 for Material Study at Extreme Conditions.

## Appendix A. Supplementary data

Supplementary data associated with this article can be found, in the online version, at doi:10.1016/j.epsl.2006.10.020.

## References

[1] J.G. Schiling, M.B. Bergeron, R. Evans, Halogens in the mantle beneath the North Atlantic, Philos. Trans. R. Soc. Lond., A 297 (1980) 147–178.

[2] S.Y. O'Reilly, W.L. Griffin, Mantle metasomatism beneath western Victoria, Australia: I. Metasomatic processes in Cr-diopside lherzolites, Geochim. Cosmochim. Acta 52 (1988) 433–447.

[3] R.L. Hervig, J.V. Smith, Dolomite–apatite inclusion in chrome–diopside crystal, Bellsbank kimberlite, South Africa, Am. Mineral. 66 (1981) 346–349.

[4] R.A. Exley, J.V. Smith, The role of apatite in mantle enrichment processes and in the petrogenesis some alkali basalt suits, Geochim. Cosmochim. Acta 46 (1982) 1375–1384.

[5] J.V. Smith, J.S. Delaney, R.L. Hervig, J.B. Dawson, F and Cl in the upper mantle: geochemical implication, Lithos 14 (1981) 133–147.

[6] M.L. Frezzotti, T. Andersen, E.-R. Neumann, S.L. Simonsen, Carbonatite melt — $CO_2$ inclusions in mantle xenoliths from Tenerife, Canary Islands: story of trapping, immiscibility and fluid-rock interaction in the upper mantle, Lithos 64 (2002) 77–96.

[7] A.E. Ringwood, S.E. Kesson, W. Hiberson, N. Ware, Origin of kimberlites and related magmas, Earth Planet. Sci. Lett. 113 (1992) 521–538.

[8] S.E. Haggerty, Superkimberlites: a geodynamic diamond window to the Earth's core, Earth Planet. Sci. Lett. 122 (1994) 57–69.

[9] D.I. Pavlov, I.P. Ilupin, Halite in the Yakutian kimberlites, its relations to serpentine, and problem of the source of depositing brines, Dokl. Akad. Nauk 213 (1973) 1406–1409.

[10] A.V. Golovin, V.V. Sharygin, N.P. Pokhilenko, V.G. Malkovets, B.A. Kolesov, N.V. Sobolev, Secondary melt inclusions in olivine from unaltered kimberlites of the Udachnaya–East Pipe, Yakutia, Dokl. Akad. Nauk 388 (2003) 93–97.

[11] R. Maas, M.B. Kamenetsky, A.V. Sobolev, V.S. Kamenetsky, N.V. Sobolev, Sr, Nd, and Pb isotope evidence for a mantle origin of alkali chlorides and carbonates in the Udachnaya kimberlite, Siberia, Geology 33 (2005) 549–552.

[12] M.B. Kamenetsky, A.V. Sobolev, V.S. Kamenetsky, R. Maas, L.V. Danyushevsky, R. Thomas, N.P. Pokhilenko, N.V. Sobolev, Kimberlite melts rich in alkali chlorides and carbonates: A potent metasomatic agent in the mantle, Geology 32 (2004) 845–848.

[13] J.D. Webster, B. De Vivo, Experimental and modeled solubilities of chlorine in aluminosilicate melts, consequences of magma evolution, and implications for exsolution of hydrous chloride melt at Mt. Somma-Visuvius, Am. Mineral. 87 (2002) 1046–1061.

[14] J.D. Webster, R.J. Kinzler, E.A. Mathez, Chloride and water solubility in basalt and andesite melts and implication for magmatic degassing, Geochim. Cosmochim. Acta 63 (1999) 729–738.

[15] M. Prinz, D.V. Manson, P.F. Hlava, K. Keil, Inclusions in diamonds: garnet lherzolite and eclogite assemblages, Phys. Chem. Earth 9 (1975) 797–815.

[16] G.P. Bulanova, P.G. Novgorodov, L.A. Pavlova, First finding of melt inclusion in diamond of the "Mir" pipe, Geochem. Int. (1988) 756–765.

[17] G.P. Bulanova, Yu.P. Barashkov, S.B. Tal'nikova, G.B. Smelova, Natural Diamond — Genetic Aspect, Nauka, Novosibirsk, 1993.

[18] G.P. Bulanova, W.L. Griffin, C.G. Ryan, Nucleation environment of diamonds from Yakutian kimberlites, Mineral. Mag. 62 (1998) 409–419.

[19] P.G. Novgorodov, G.P. Bulanova, L.A. Pavlova, V.N. Mikhailov, V.V. Ugarov, A.P. Shebanin, K.P. Argunov, Inclusions of potassic phases, coesite and omphacite in the coated diamond crystal from the "Mir" pipe, Dokl. Akad. Nauk 310 (1990) 439–443.

[20] W. Wang, T.M. Moses, J.E. Shigley, Physical and chemical features of large coated natural diamond crystal, Diamond Relat. Mater. 12 (2003) 330–335.

[21] O. Navon, I.D. Hitcheon, G.R. Rossman, G.J. Wasserburg, Mantle-derived fluids in diamond microinclusions, Nature 325 (1988) 784–789.
[22] M. Schrauder, O. Navon, Hydrous and carbonatitic mantle fluids in fibrous diamonds from Jwaneng, Botswana, Geochim. Cosmochim. Acta 58 (1994) 761–771.
[23] M. Schrauder, O. Navon, D. Szafranek, F. Kaminsky, E. Galimov, Fluids in Yakutian and Indian diamonds, Mineral. Mag. 58A (1994) 813–814.
[24] M. Schrauder, C. Koeberl, O. Navon, Trace element analyses of fluid-bearing diamonds from Jwaneng, Botswana, Geochim. Cosmochim. Acta 60 (1996) 4711–4724.
[25] O. Klein-BenDavid, A.M. Longvinova, E.S. Izraeli, N.V. Sobolev, O. Navon, Sulfide melt inclusions in Yubileinayan (Yakutia) diamonds, 8th Inernational Kimberlite Conference Long Abstract, 2003, p. FLA_0111.
[26] E.S. Izraeli, J.W. Harris, O. Navon, Mineral inclusions in cloudy diamonds from Koffiefontein, South Africa, 8th Inernational Kimberlite Conference Long Abstract, 2003, p. FLA_0113.
[27] A.A. Shiryaev, E.S. Izraeli, E.H. Hauri, O.D. Zakharchenko, O. Navon, Chemical, optical and isotopic investigation of fibrous diamonds from Brazil, Russ. Geol. Geophys. 46 (2005) 1185–1201.
[28] A.M. Logvinova, O. Klein-BenDavid, E.S. Izraeli, O. Navon, N.V. Sobolev, Microinclusions in fibrous diamonds from Yubileinaya kimberlite pipe (Yakutia), 8th Inernational Kimberlite Conference Long Abstract, 2003, p. FLA_0025.
[29] O. Klein-BenDavid, E.S. Izraeli, E. Hauri, O. Navon, Mantle fluid evolution — a tale of one diamond, Lithos 77 (2004) 243–253.
[30] O. Klein-BenDavid, R. Wirth, O. Navon, TEM imaging and analysis of microinclusions in diamonds: a close look at diamond-bearing fluids, Am. Mineral. 91 (2006) 353–356.
[31] F. Chen, J. Guo, C. Chen, C. Liu, High-K and high-Cl inclusions in diamond and mantle metasomatism, Acta Mineral. Sin. 12 (1992) 193–198.
[32] E.S. Izraeli, J.W. Harris, O. Navon, Brine inclusions in diamonds: a new upper mantle fluid, Earth Planet. Sci. Lett. 5807 (2001) 1–10.
[33] E.S. Izraeli, J.W. Harris, O. Navon, Fluid and mineral inclusions in cloudy diamonds from Koffiefontein, South Africa, Geochim. Cosmochim. Acta 68 (2004) 2561–2575.
[34] G. Turner, R. Burgess, M. Bannon, Volatile-rich mantle fluids inferred from inclusions in diamonds and mantle xenoliths, Nature 334 (1990) 653–655.
[35] L.H. Johnson, R. Burgess, G. Turner, H.J. Milledge, J.W. Harris, Noble gas and halogen geochemistry of mantle fluids: comparison of African and Canadian diamonds, Geochim. Cosmochim. Acta 64 (2000) 717–732.
[36] R. Burgess, G. Turner, Halogen geochemistry of mantle fluids in diamonds, in: K.A. Farley (Ed.), Volatiles in the Earth and Solar system, Proc. AIP Conf., vol. 341, 1995, pp. 91–98.
[37] O. Navon, E.S. Izraeli, O. Klein-BenDavid, Fluid inclusions in diamonds — the carbonatitic connection, 8th Inernational Kimberlite Conference Long Abstract, 2003, p. FLA_0107.
[38] O. Klein-BenDavid, R. Wirth, E.S. Izraeli, O. Navon, Brine rich diamond-forming fluids, EOS Trans. AGU Fall Meet, vol. Suppl 85, 2004, p. V33F_O2.
[39] L.L. Perchuk, O.G. Safonov, V.O. Yapaskurt, J.M. Barton Jr., Crystal-melt equilibria involving potassium-bearing clinopyroxene as indicators of mantle-derived ultrahigh-potassic liquids: an analytical review, Lithos 60 (2002) 89–111.
[40] I.C. Freestone, D.L. Hamilton, The role of liquid immiscibility in the genesis of carbonatites — an experimental study, Contrib. Mineral. Petrol. 73 (1980) 105–117.
[41] N.I. Suk, Experimental study of liquid immiscibility in silicate–carbonate systems, Petrology 9 (2001) 477–488.
[42] N.I. Suk, Experimental study of the genesis of carbonatite deposits, in: V.A. Zharikov, V.V. Fedkin (Eds.), Experimental Mineralogy: Some Results on the Century's Frontiers, vol. 1, Nauka, Moscow, 2004, pp. 327–344.
[43] Yu.A. Litvin, Physical and Chemical Studies of Melting of Materials from the Deep Earth, Nauka, Moscow, 1991.
[44] O.G. Safonov, Yu.A. Matveev, Yu.A. Litvin, L.L. Perchuk, Experimental study of some joins of the system $CaMgSi_2O_6$–$(Ca,Mg)_3Al_2Si_3O_{12}$–$KAlSi_2O_6$–$K_2(Ca,Mg)(CO_3)_2$ at 5–7 GPa in relation to the genesis of garnet–clinopyroxene–carbonate rocks of the Kokchetav Complex (Northern Kazakhstan), Petrology 10 (2002) 519–539.
[45] O.G. Safonov, Yu.A. Litvin, L.L. Perchuk, L. Bindi, S. Menchetti, Phase relations of potassium-bearing clinopyroxene in the system $CaMgSi_2O_6$–$KAlSi_2O_6$ at 7 GPa, Contrib. Mineral. Petrol. 146 (2003) 120–133.
[46] M. Eremets, High Pressure Experimental Methods, Oxford Univ. Press, Oxford, 1996.
[47] C.G. Homan, Phase diagram of Bi up to 140 kbars, J. Phys. Chem. Solids 36 (1975) 1249–1254.
[48] C.S. Kennedy, G.C. Kennedy, The equilibrium boundary between graphite and diamond, J. Geophys. Res. 81 (1976) 2467–2470.
[49] A.V. Spivak, Yu.A. Litvin, Diamond synthesis in multicomponent carbonate–carbon melts of natural chemistry: elementary process and properties, Diamond Relat. Mater. 13 (2004) 482–487.
[50] J.A. Dalton, D.C. Presnall, The Continuum of Primary Carbonatitic-Kimberlitic Melt Compositions in Equilibrium with Lherzolite: Data from the System CaO–MgO–$Al_2O_3$–$SiO_2$–$CO_2$ at 6 GPa, J. Petrol. 39 (1998) 1953–1964.
[51] A.V. Girnis, V.K. Bulatov, G.P. Brey, Transition from kimberlite to carbonatite melt under mantle Parameters: an experimental study, Petrology 13 (2005) 1–15.
[52] R.A. Brooker, The effect of $CO_2$ saturation on immiscibility between silicate and carbonate liquids: an experimental study, J. Petrol. 39 (1998) 1905–1915.
[53] W.-J. Lee, P.J. Wyllie, Liquid immiscibility between nephelinite and carbonatite from 1.0 to 2.5 GPa compared with mantle melt compositions, Contrib. Mineral. Petrol. 127 (1997) 1–16.
[54] W.-J. Lee, P.J. Wyllie, G.R. Rossman, $CO_2$-rich glass, round calcite crystals, and no liquid immiscibility in the system CaO–$SiO_2$–$CO_2$ at 2.5 GPa, Am. Mineral. 79 (1994) 1135–1144.
[55] Y. Dessureault, J. Sangster, A.D. Pelton, Coupled phase diagram-thermodynamic analysis of the 24 binary systems $A_2CO_3$–AX and $A_2SO_4$–AX where A = Li, Na, K and X = Cl, F, $NO_3$, OH, J. Phys. Chem. Ref. Data 19 (1990) 1149–1178.
[56] P.J. Wyllie, I.D. Ryabchikov, Volatile components, magmas, and critical fluids in upwelling mantle, J. Petrol. 41 (2000) 1195–1206.
[57] K.R. Moore, B.J. Wood, The transition from carbonate to silicate melts in the CaO–MgO–$SiO_2$–$CO_2$ system, J. Petrol. 39 (1998) 1943–1951.
[58] G.M. Yaxley, G.P. Brey, Phase relations of carbonate-bearing eclogite assemblage from 2.5 to 5.5 GPa: implications for petrogenesis of carbonatites, Contrib. Mineral. Petrol. 146 (2004) 606–619.
[59] I.D. Ryabchikov, A.L. Boettcher, Experimental evidence at high pressure for potassic metasomatism in the mantle of the Earth, Am. Mineral. 65 (1980) 915–919.

[60] E.L. Tomlinson, E. De Schrijver, K. De Corte, A.P. Jones, L. Moens, F. Vanhaecke, Trace element compositions of submicroscopic inclusions in coated diamond: a tool for understanding diamond petrogenesis, Geochim. Cosmochim. Acta 69 (2005) 4719–4732.
[61] Yu.N. Pal'yanov, V.S. Shatsky, A.G. Sokol, A.A. Tomilenko, N.V. Sobolev, Crystallization of metamorphic diamond: an experimental modeling, Dokl. Akad. Nauk 381 (2001) 935–938.
[62] O.G. Safonov, O.A. Levykina, L.L. Perchuk, Yu.A. Litvin, Liquid immiscibility and phase equilibria in chloride–aluminosilicate melts at 4–7 GPa, Dokl. Akad. Nauk 400 (2005) 119–123.
[63] W.G. Minarik, Complications to carbonate melt mobility due to the presence of an immiscible silicate melt, J. Petrol. 39 (1998) 1965–1973.
[64] Y. Wang, H. Kanda, Growth of HPHT diamonds in alkali halides: possible effects of oxygen contamination, Diamond Relat. Mater. 7 (1998) 57–63.
[65] Yu.A. Litvin, Alkaline–chloride components in processes of diamond growth in the mantle and high-pressure experimental conditions, Dokl. Akad. Nauk 389 (2003) 388–391.
[66] E.L. Tomlinson, A.P. Jones, H.J. Milledge, High-pressure experimental growth of diamond using C–$K_2CO_3$–KCl as analogue for Cl-bearing carbonate fluid, Lithos 77 (2004) 287–294.
[67] Yu.A. Litvin, L.T. Chudinovskih, V.A. Zharikov, Crystallization of diamond and graphite in mantle alkali carbonate melts in experiment at 7–11 GPa, Dokl. Akad. Nauk 355 (1997) 679–772.
[68] Yu.N. Pal'yanov, A.G. Sokol, Yu.V. Borzdov, A.F. Khokhryakov, Fluid-bearing alkaline melts as the medium for the formation of diamonds in the Earth's mantle: an experimental study, Lithos 60 (2002) 145–159.
[69] Yu.N. Pal'yanov, A.G. Sokol, Yu.V. Borzdov, A.F. Khokhryakov, Diamond formation from the mantle carbonate fluids, Nature 400 (1999) 417–418.
[70] T. Akagi, A. Masuda, Isotopic and elemental evidence for a relationship between kimberlite and Zaire cubic diamonds, Nature 336 (1988) 665–667.